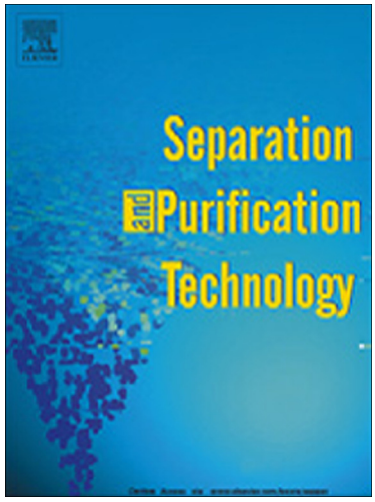

Experimental determination of the hydrodynamic forces within nanofiltration membranes and evaluation of the current theoretical descriptions

Darren L. Oatley-Radcliffe, Steffan R. Williams, Thomas J. Ainscough, Christopher Lee, Daniel J. Johnson, Paul M. Williams

PII: S1383-5866(15)30025-3
DOI: http://dx.doi.org/10.1016/j.seppur.2015.05.041
Reference: SEPPUR 12371

To appear in: *Separation and Purification Technology*

Received Date: 20 February 2015
Revised Date: 27 May 2015
Accepted Date: 28 May 2015

Please cite this article as: D.L. Oatley-Radcliffe, S.R. Williams, T.J. Ainscough, C. Lee, D.J. Johnson, P.M. Williams, Experimental determination of the hydrodynamic forces within nanofiltration membranes and evaluation of the current theoretical descriptions, *Separation and Purification Technology* (2015), doi: http://dx.doi.org/10.1016/j.seppur.2015.05.041

Experimental determination of the hydrodynamic forces within nanofiltration membranes and evaluation of the current theoretical descriptions

Darren L. Oatley-Radcliffe*, Steffan R. Williams, Thomas J. Ainscough, Christopher Lee, Daniel. J. Johnson, Paul M. Williams

Centre for Water Advanced Technologies and Environmental Research (CWATER), College of Engineering, Swansea University, Singleton Park, Swansea SA2 8PP, UK.

* to whom correspondence should be addressed
Tel: + 44 (0)1792 606 668
Email address: d.l.oatley@swansea.ac.uk

Keywords: hindrance factors, hydrodynamic, Nanofiltration, characterisation

Abstract

In this study a series of different molecular weight PEG solutions have been characterised for particle size and the results have been used, in conjunction with several other techniques, to determine the pore size of the Nadir UH004 membrane. The resulting information, in conjunction with experimentally determined rejection profiles for the PEG solutions, has then been used to back calculate the hindrance factors for nanofiltration rejection theory. These experimentally derived values obtained for the hindrance factors were found to be in close agreement with the widely accepted theoretical predictions derived from hydrodynamic theory for micro and ultrafiltration. To our knowledge, this is the first experimental validation of these hindrance factors for nanofiltration and suggests that the correlations found throughout the literature are accurate enough for the calculation of hindrance factors describing the hydrodynamic drag forces experienced by a solute inside a nanopore.

1.0 Introduction

Membrane based processes for the separation and concentration of valuable compounds have received significant attention in the past three decades and the future remains promising with significant growth expected. The driving factors for growth in membrane technologies are attributed to the ease of operation and scale up, low operational cost, low energy requirement and high selectivity factors [1]. Nanofiltration (NF) is a pressure driven membrane separation technique situated between ultrafiltration and reverse osmosis. NF membranes are typically polymeric, asymmetric and consist of a low resistance support layer with a functionally active porous top layer [2, 3]. The nominal molecular weight cut-off of an NF membrane is in the range 100-1000 Da, indicating that the NF membrane active layer has an approximate pore size of 1 nm.

NF is an extremely complex process and is dependent on the micro-hydrodynamic and interfacial events occurring at the membrane surface and within the membrane nanopores. The nano-scale phenomena involved in neutral and charged solute separations by NF are extremely complex and, as such, are likely to be a rigorous test of any macroscopic description of ion transport and partitioning. The optimisation of NF membrane equipment along with an expansion in potential applications would be greatly facilitated if simple, accurate and quantitative methods for predicting process

performance were available. An ideal method would combine the physical property data of a given process stream and a membrane along with a fundamental mathematical description of the transport processes so that the required optimum separation conditions could be determined. However, the near atomic length scales of the nanofiltration process leads to inherent problems when considering existing macroscopic descriptions of hydrodynamics and solute-pore interactions [4].

Solutes moving in free solution experience drag forces exerted by the solvent flowing through the confined pore structure. The movement of solutes in this confined space is greatly affected by the local environment and the transport of the solute is considered as hindered. Hindered transport can be expressed in terms of both a convective and diffusive element which contributes to the overall transport effect. Theories describing hindered transport have received attention since the mid 1900's, with most considering biological applications [5]. This early work utilised equivalent pore analysis to describe lipid-insoluble permeation of capillary endothelial walls, red blood cells and the nuclear envelope of eukaryotic cells as well as artificial membranes in terms of movement in water filled pores [6].

The effective diffusion coefficient of a solute within a pore of similar size is usually lower than that of the bulk solution due to the confinement [7]. Diffusion through pores is also hindered due to the irregular pore structure; current descriptions of this phenomena assume a perfectly cylindrical pore, however, in reality the pore structure is most likely far from perfectly cylindrical. Restricted pore diffusion has been studied for decades and indicates that hindered diffusivity is smaller than that of the diffusivity of the free solution [8]. The scale of nanopores would suggest that the description of diffusion is definitely hindered and is likely to deviate in a similar fashion to that of Knudsen diffusion. Knudsen diffusion considers the diffusion of a gas molecule through a small nano-scale pore, however, the spacial confinement of a nanopore would physically allow the transport of only single solutes and solvents at a time. The convective hindrance factor, K_c, describes the effects that flow of the solvent in the confines of the pore (including wall effects) has on the solute being transported and represents the ratio of solute velocity to solvent velocity in the pore. The diffusive hindrance factor, K_d, represents the ratio of the hindered diffusivity of the solute in the pore to that of the bulk solution. The values for these convective and diffusive drag forces in membrane pores are usually calculated from complex hydrodynamic flow equations using finite element techniques [9-11]. To the best knowledge of the authors there are no experimentally derived correlations relating real experimental data to hydrodynamic drag in cylindrical pores of nano-scale dimensions. Dechadilok and Deen [12] listed a number of studies involving the microscopic visualization of the motion of individual particles in slit-like pores. Despite the obvious difference between a slit and an assumed cylindrical nano-pore, the scale of the solutes and pores listed are orders of magnitude greater than those found in a nanofiltration membrane separation.

The aim of this work is to experimentally determine the convective and diffusive hindrance factors associated with the transport of solutes in nanopores and then make a comparison of these experimentally derived hydrodynamic factors to those obtained by theoretical means. This will facilitate the validation of such theoretical descriptions for NF membrane processes and will confirm that the models in use are a true representation of the complex phenomena occurring in the real separation process. The experimental work will study transport performance of a polymeric membrane with a series of polyethyleneglycols (PEGs) of differing molecular weight. PEG is a neutral

solute which negates the charge separation mechanism of the NF membrane and significantly reduces the complexity of the Nernst-Planck equation simplifying the calculation of the hindrance factors from rejection data.

2.0 Relevant Theory

A solute moving in a solution experiences a resistance or drag force from the solvent. The magnitude of the drag force exerted on a particular solute is dependent on the shape and size of the solute as well as the viscosity of the solvent. In the case of a spherical solute in dilute bulk solution the drag force experienced may be expressed as:

$$F_\infty = (6\pi\eta r_s)u_s \quad (1)$$

where F_∞ is the drag force in the bulk solution, η is the solvent viscosity, r_s is the radius of the solute and u_s is the solute velocity. In the case where the solute is much larger than the solvent the Stokes-Einstein equation may be applied which relates the diffusion coefficient of the solute in the bulk solution, $D_{i,\infty}$, to that of the Stokes-Einstein radius of the solute, r_s [5]:

$$r_s = \frac{kT}{6\pi\eta D_{i,\infty}} \quad (2)$$

where k is the Boltzmann's constant and T is the absolute temperature.

Similar hydrodynamic constraints are applicable for the convective transport of a solute through pores, therefore eqns. (1) and (2) can be adapted to describe the drag force experienced by a solute when moving in a pore.

Hindrance (or drag) factors are introduced into the NF models to account for the hindered passage of solutes through the confined polymer structure of the NF membrane. The hindrance factors for movement inside an interconnecting network of polymers are difficult to derive and have not been reported so far. Therefore, all of the work in this area to date has assumed a solute of rigid spherical shape moving through a perfectly cylindrical pore of infinite length as shown in Figure 1. The solute with radius r_s is moving with velocity u_s in the direction x along the centreline of the cylindrical pore of radius r_p and length Δx. For such a case, expressions for the hindrance factors can be derived theoretically from a fundamental knowledge of the system hydrodynamics [5]. The derivation of hindrance factor expressions require the following basic assumptions:

I. The radius of the pore r_p and solute molecule r_s greatly exceed that of the solvent.
II. Pore flow is fully developed with a very low Reynolds number one pore radius downstream of the pore entrance.
III. Mass transfer effects are neglected at the pore entrance and exit.
IV. The bulk solution is assumed to be sufficiently dilute to minimise all solute-solute interactions.

When the flow is assumed to be at an isothermal condition, the drag force experienced by the solute is exactly balanced by hydrodynamic forces to give:

$$-kT\ \frac{\delta \ln c}{\delta x} - 6\pi\eta r_s K(u_s - Gu_x) = 0 \quad (3)$$

where u_x is the unperturbed fluid velocity upstream or downstream of the particle, c is the concentration, K is the hydrodynamic coefficient and G is the lag coefficient, accounting for the effects of the finite pore size. In an unbounded fluid, $K = G = 1$ and the second term is equivalent to Stokes' Law (eqn. 1). The left hand term of eqn. (3) represents the diffusional force per solute in the x direction and the right hand term corresponds to the hydrodynamic forces.

Defining solute flux as $J_s = u_s c$ allows eqn. (3) to be rearranged resulting in:

$$J_s = -K^{-1}D_\infty \frac{\delta c}{\delta x} + Gu_x c \quad (4)$$

Eqn. (4) is the standard flux expression for a dilute liquid solution and accounts for the contribution of convection and diffusion modified by the factors G (a lag coefficient) and K^{-1} (an enhanced drag coefficient) respectively. These drag coefficients are dependent on the ratio of solute radius, r_s, to the pore radius, r_p, usually expressed as:

$$\lambda = \frac{r_s}{r_p} \quad (5)$$

The assumption of a long cylindrical pore results in the unperturbed fluid velocity having a parabolic profile given as:

$$u_x = 2\hat{u}_x(1 - \beta^2) \quad (6)$$

where $\hat{u}_x$ is the average solvent velocity over the pore cross section and $\beta = \frac{r}{r_p}$ (a dimensionless radial position). The subsequent average solute flux $\hat{J}_s$ over the pore cross section is expressed as:

$$\hat{J}_s = \frac{\int_0^1 J_s\, \beta d\beta}{\int_0^1 \beta d\beta} = 2\int_0^{1-\lambda} J_s\, \beta d\beta \quad (7)$$

Substitution of eqn. (4) into eqn. (7) results in:

$$\hat{J}_s = -2D_\infty \int_0^{1-\lambda} K^{-1}\ \frac{\delta c}{\delta x}\ \beta d\beta + 4\,\hat{u}_x \int_0^{1-\lambda} Gc(1-\beta^2)\beta d\beta \quad (8)$$

The concentration term, c, may be approximated by:

$$c = g(x)\exp^{-\frac{E(\beta)}{kT}} \quad (9)$$

where $g(x)$is the function describing the variation in axial concentrations within the pore and E is the term describing the electrostatic interactions. Combining eqns. (8) and (9) results in the final local flux equation, given as:

$$\hat{J}_s = -K_d D_\infty \frac{d\hat{c}}{dx} + K_c \hat{u}_x\, \hat{c} \quad (10)$$

where K_d and K_c are the integral of inverse enhanced drag and the lag coefficient respectively.

K_d is then described as:

$$K_d = \frac{\int_0^{1-\lambda} K^{-1} exp^{-E/kT}\, \beta d\beta}{\int_0^{1-\lambda} exp^{-E/kT}\, \beta d\beta} \quad (11)$$

and K_c is defined as:

$$K_c = \frac{2\int_0^{1-\lambda} G(1-\beta^2)\, exp^{-E/kT}\, \beta d\beta}{\int_0^{1-\lambda} exp^{-E/kT}\, \beta d\beta} \quad (12)$$

The partitioning coefficient (ratio of the average intrapore concentration to that of the bulk solution), ϕ, was defined by Deen [5] for the boundary conditions $x = 0,\ g(0) = C_o$ and when $X = \Delta x,\ g(L) = C_{\Delta x}$ as:

$$\phi = \frac{\hat{C_0}}{C_0} = \frac{\hat{C_L}}{C_L} = 2\int_0^{1-\lambda} exp^{-E/kT}\, \beta d\beta \quad (13)$$

where C_0 and C_L are the solute concentrations in the external solution adjacent to the membrane surface. However in the case of a neutral solute and for purely steric interactions between the solute and the pore wall ($E = 0$), the partitioning coefficient then reduces to:

$$\phi = (1 - \lambda)^2 \quad (14)$$

The integration of eqn. (11) with the same boundary conditions of eqn. (13) leads to the macroscopic flux equation:

$$\hat{J}_s = W\, \hat{u}_x C_0 \frac{[1 - (C_L/C_0) exp^{-Pe}]}{[1 - exp^{-Pe}]} \quad (15)$$

where W is defined as:

$$W = \phi K_c = 4\int_0^{1-\lambda} G(1-\beta^2) exp^{-E/kT}\, \beta d\beta \quad (16)$$

and Pe is the Peclet number based on pore length described as:

$$Pe = \frac{W\, \hat{u}_x\, \Delta x}{H\, D_\infty} \quad (17)$$

with H defined as:

$$H = \phi K_d = 2\int_0^{1-\lambda} K^{-1} exp^{-E/kT}\, \beta d\beta \quad (18)$$

In the case of neutral solutes $E = 0$. Rearranging eqns. (16) and (17) for K_c and K_d respectively for cylindrical pores gives:

$$K_c(\lambda) = \frac{4}{(1-\lambda)^2} \int_0^{1-\lambda} G(\lambda, \beta)(1 - \beta^2)\, \beta d\beta \quad (19)$$

$$K_d(\lambda) = \frac{2}{(1-\lambda)^2} \int_0^{1-\lambda} \frac{\beta d\beta}{K(\lambda,\beta)} \quad (20)$$

The limits of eqn. (15) are as follows:

$$\hat{J}_s = \frac{HD_\infty}{\Delta x} (C_0 - C_{\Delta x}) \qquad (Pe < 1) \quad (21)$$

$$\hat{J}_s = W\,\hat{u}_x C_0 \quad (P > 1) \tag{22}$$

where solute transport is dominated by diffusion when $Pe < 1$ and by convection when $Pe > 1$.

Studies have demonstrated that a centreline approximation for the solute location in the nanopore provides an accurate estimation of the hydrodynamic coefficients [4]. Thus, for an uncharged interaction where $E = 0$, a Hagen-Poiseuille velocity profile and the centreline approximation results in eqn. (16) and (18) becoming:

$$K_{i,c} = \frac{u_s}{u_x} = (2 - \phi_i)G(\lambda, 0) \tag{23}$$

$$K_{i,d} = \frac{D_{i,p}}{D_{i,\infty}} = K^{-1}(\lambda, 0) \tag{24}$$

where $D_{i,p}$ is the hindered diffusivity inside the NF pore, u_s is the solute velocity and u_x is the maximum solvent velocity.

The pore radius of an NF membrane is very small and as a direct consequence the solute velocity profile may not be fully developed. In such a case where a homogeneous velocity profile is more appropriate $K_{i,c}$reduces to [13]:

$$K_{i,c} = G(\lambda, 0) \tag{25}$$

A review of the theoretical calculations for the determination of the hindrance factors has been conducted [5, 12] and point value solutions calculated using finite element methods are available for the hindrance factors, provided in Table 1. Several authors have fitted polynomial expressions to these point values and these are summarised, along with the valid range, in Table 2. Figure 2 illustrates these point values for hindrance factors and demonstrates the polynomial fitting expression of Oatley [14] as an example. Table 2 indicates that there are many alternative expressions derived for the simple calculation of the hindrance factors. These models all assume centreline positioning of the particle, however, the model produced by Dechadilok and Deen [12] averaged the properties of the convective and diffusive forces across the pore cross section for cylindrical pores. Silva et al. [11] produced similar plots to that in Figure 2 but extrapolated beyond the limits of validity for many of the proposed expressions. Essentially, any of these expressions may be used to calculate the magnitude of the hindrance factors so long as the calculation and model in use are within the determined valid range. The authors would recommend the model proposed by Oatley [14] as this spans the maximum range of λ, particularly important when modelling NF pore size distributions.

The transport of ions through a nanofiltration membrane is typically described using the extended Nernst-Planck equation:

$$j_i = -\frac{c_i K_{i,d} D_{i,\infty}}{RT}\frac{d\mu}{dx} + K_{i,c} c_i V \tag{26}$$

where j_i is the ionic flux, c is the concentration, V is the solvent velocity and $K_{i,c}$ and $K_{i,d}$ are the hindrance factors to account for the convection and diffusion in the confined NF pore.

For a neutral species, the solution of eqn. (26) is much simplified and leads to an analytical expression to calculate rejection as [15, 16]:

$$R = 1 - \frac{C_{i,p}}{C_{i,w}} = 1 - \frac{K_{i,c}\phi_i}{1-[1-\phi_i K_{i,c}]exp(-Pe')} \quad (27)$$

where $Pe' = \frac{K_{i,c}}{K_{i,d}}\frac{r_p^2}{8\eta D_{i,\infty}}\Delta P_e$ is a modified Peclet number and ΔP_e is the effective pressure driving force ($\Delta P - \Delta\Pi$). At limiting rejection, where $\Delta P_e \to \infty$, this expression simplifies further to yield:

$$R_i = 1 - K_{i,c}\phi_i \quad (28)$$

The rejection in eqn. (28) is dependent only upon λ (ratio of solute to pore radius) and the hindrance coefficient $K_{i,c}$. Therefore, from a knowledge of the membrane pore size, the solute size and the experimental limiting rejection, the hindrance factor $K_{i,c}$ may be calculated. Then, with the values mentioned and experimental rejection determined over a full range of pressure (low pressure to high pressure, typically 0 to 30 bar) $K_{i,d}$ can be calculated.

3.0 Materials and Methods

3.1 Particle Sizing (ZetaSizer)

Particle size for the PEG solutions was determined using a Zetasizer (Nano ZS, Malvern Instruments, Malvern, Worces., UK.). Samples were prepared using deionised water and were filtered with a 0.22 µm syringe driven filter unit (Millipore U.K Ltd.) into a 4.0 mL glass cuvette (Malvern Instruments, Malvern, Worces., UK) for ZetaSizer measurements. The method and number of measurements performed was selected in accordance to a British Standard [17]. For a particle size of less than 10 nm, a concentration greater than 0.5 g/litre is recommended with no upper limit providing the material exhibits no aggregation or gelation. In total eight PEGs (Polyethylene glycol, molecular weights: 200, 400, 600, 1000, 1450, 2000, 3400, 4600) were used and obtained in high purity form from Sigma Aldrich (Dorset, UK). In this study a concentration of 4 g/litre was used in all cases except for molecular weights below 600 where a concentration of 10 g/litre was used in order to improve measurement intensity and count rate. The data obtained was compared to literature values where possible and theoretical models for validation.

3.2 Brunauer-Emmett-Teller (BET) nitrogen adsorption

BET analysis is commonly used for measuring membrane structural characteristics, particularly surface area of the membrane and also pore size distribution using the gas adsoprtion-desorption (GAD) technique [18-20]. Pore size measurements were determined using a Quantachrome Nova

2000e surface area analyser (Quantachrome UK Ltd., Hook, UK). The measurement technique of this instrument is based on physisorption and desorption of a gas, nitrogen in this case, at the surface and inside the pores of the sample. Prior to analysis, the two membrane samples were prepared by degassing under vacuum at 50°C for 48 hours until a constant weight was obtained. The weight of the dry sample and sample tube were determined using an analytical balance. In order to determine the sample properties, the sample cell is placed under vacuum and immersed in liquid nitrogen; a known flux of nitrogen is then introduced to the cell while simultaneously measuring the pressure. The Horvath-Kawazoe (HK) method [20] was used to calculate the pore size distribution from the low relative pressure region of the adsorption isotherm. The HK method is derived independently from the Kelvin equation and expresses the adsorption potential function within slit-like micropores as a function of the effective pore width. By selecting effective pore widths in the micropore range, the HK equation can be used to calculate the corresponding relative pressures. Then, from the adsorption isotherm, the amount of adsorption at each of these relative pressures is determined. Differentiation of the volume of gas adsorbed relative to the total uptake with respect to the effective pore width yields a pore size distribution in the micropore range [38]. The t-plot function, volume of gas adsorbed versus time and is a statistical measure of the thickness of an adsorbed film, in this case was determined using a t curve derived for carbon blacks and uses the de Boer's method [39,40]. These calculations are conducted automatically by the Quantachrome software.

3.3 Atomic-Force Microscopy (AFM) measurements

Membrane pores size was also determined using AFM and measurements were performed on a Multimode AFM with Nanoscope IIIa controller (Bruker, USA) using manufacturer supplied software. All measurements were carried out using tapping mode under ambient laboratory conditions (humidity ~60%, temperature ~22°C) or in high purity water (resistivity 18.2 MΩ s) using TESP tapping mode levers for measurements in air (Bruker, nominal spring constant 20-80 N/m) and contact mode NP-S levers for measurements in liquid (Bruker, nominal spring constant 0.12 N/m). Data was analysed using the instrument control software (NanoScope software version 5.31R1) directly from the z-scan data. The particle size analysis feature of the AFM software was employed to measure the size of surface pores. This software facilitates the measurement of features sited higher than an arbitrary threshold set by the user. To measure the size of channels (interpreted as pores) negative thresholding was selected. As the value of the threshold used is arbitrary, a value of 0 was employed in all studies, i.e. the mean plane for the image was used as the baseline. The software then generated data for the mean diameter, mean area (along with standard deviations) and count number for the channels, i.e. for all features identified as being below the threshold. By multiplying the mean area by the count number the total surface area of the pores in the image was estimated and porosity was determined as a percentage of the total surface of the image occupied by pores.

3.4 Membranes and equipment set up

All rejection experiments were carried out at laboratory scale using a frontal filtration set-up illustrated in Figure 3. The system consisted of a customised membrane cell supplied by Membranology (Membranology Ltd., Swansea, UK). The active membrane area in the cell is 0.00418 m^2. The Nadir UH004 membrane was used for the investigation which has a reported MWCO (molecular weight cut off) of 4000 (Microdyn Nadir, Germany). Membranes were cut to size and immersed overnight in ultra-pure water in darkness at 3 °C. Sucrose and the same eight PEGs (see

section 3.1) were obtained in high purity form from Sigma Aldrich (Dorset, UK) and a feed concentration of 600 mg/L for each PEG solution was maintained throughout the experimental work. Similarly for the sucrose solution. Ultra pure reverse osmosis water was obtained from an Elix3® Essential water purification system supplied by Millipore UK Ltd. (Watford, UK). The cell was operated at 1, 3, 5, 10, 15, 20, 25 and 30 bar applied pressure with a stirrer speed set to 300 rpm (previously determined as optimum to account for mass transfer effects [16].

Prior to starting experimentation, the membrane was pressurised for 1 hr at 30 bar with ultra-pure water. The applied pressure for the cell was adjusted via a regulator connected to oxygen free nitrogen (BOC, UK) and monitored using a pressure sensor (Druck DPI 104, RS Components, UK). All membrane experiments were carried out at 25 °C maintained by a water bath. Permeate flow was measured via the mass output of the cell monitored by a balance (Ohaus Navigator N24120, Ohaus Europe, Switzerland) and recorded by a PC using WinWedge software (TAL Technologies, Pennsylvania), taking readings at 15 second intervals. The first 10 mL of permeate obtained was sent to waste in order to account for equipment hold up followed by the collection of a 10 mL permeate sample for analysis. This ensured that the cell contents variation over the duration of the experiment varied no more than 10% and this variation was neglected from calculations. Each experiment was conducted at least three times and the average result is reported.

Sample analysis of PEG was carried out using a Varian Prostar 350 Refractive Index Detector (Agilent Technologies, Wokingham, UK). The PEG solutions were pumped through the detector using an Agilent 1100 (Agilent Technologies, UK) HPLC Pump and the signal generated was recorded. This signal value was then converted to the permeate PEG concentration by comparison to a calibration curve of known concentration. Sucrose analysis was carried out using a Shimadzu TOC-L CPH analyser (Shimadzu UK Ltd. Milton Keynes, UK) according to the manufacturer instructions.

The experimental rejection characteristics of a membrane are typically defined by observed rejection [21]:

$$R_{obs} = 1 - \frac{C_p}{C_F} \tag{29}$$

where C_P and C_F are the concentrations of the permeate and feed respectively. In reality, due to concentration polarisation this definition of rejection is not accurate because the concentration at the membrane surface, C_W is higher than that of the bulk feed concentration, C_f. The real rejection of the solute, R, which is always equal to or greater than R_{obs} is defined as:

$$R_{real} = 1 - \frac{C_p}{C_w} \tag{30}$$

The concentration at the wall, C_W, is extremely difficult to measure directly and therefore is normally calculated indirectly using a suitable model for concentration polarisation [22]. In order to account for the concentration polarisation effect the infinite rejection method [23] is used combined with the mass transfer characteristics of the membrane equipment, *k*, (previously determined by Oatley-Radcliffe et al. [16]) resulting in:

$$ln\left(\frac{1-R_{obs}}{R_{obs}}\right) = \frac{J_v}{k} + ln\left(\frac{1-R_{real}}{R_{real}}\right) \tag{31}$$

In this case, the mass transfer coefficient may be represented as

$$k = a\omega^n \tag{32}$$

where a = 2.87x10^{-06} and n = 0.415. The real rejection can be calculated by rearranging of eqn. (31) to yield:

$$R_{real} = \frac{1}{Exp\left(ln\left[\frac{1-R_{obs}}{R_{obs}}\right] - \frac{J_v}{a\omega^n}\right) + 1} \tag{33}$$

In order to calculate the hindrance factor $K_{i,c}$, the limiting rejection of each PEG studied must be obtained from the experimental data and to do this a statistical expression was fitted to the data in order to obtain a definitive value. The expression used was an exponential to maximum with two parameters, i.e.

$$f = a\left(1 - exp^{(-bx)}\right) \tag{34}$$

where a and b are fitting parameters.

The experimental data was regressed using the statistical relationship in order to obtain a maximum coefficient of determination.

4.0 Results & Discussion

4.1 Particle Sizing

The values for particle size obtained from the zetasizer were compared to current models and literature values for various small solutes in order to gain an understanding of the accuracy and validity of the equipment and current predictive models for particle size.

The predictive models used in this study were those of:

Combe et al. [24], derived an expression to predict solute radius from the diffusion coefficients of various forms of PEG using four PEG varieties (MW = 300, 600, 3350 and 10,000):

$$r_s = 0.045MW^{0.44} \tag{35}$$

Singh et al [25], developed an expression for PEG solute radius directly from intrinsic viscosity data:

$$r_s = 16.73 \times 10^{-10} MW^{0.557} \tag{36}$$

Bowen and Mohammad [26], developed and expression to predict small molecule radius from known values for standard materials (such as glycerine, glucose, sucrose, raffinose, α-cyclodextrin, and vitamin B12).

$$\log_{10} r_s = -1.3363 + 0.395 \log_{10} MW \tag{37}$$

Where r_s is the solute radius and MW is the molecular weight of the species in each case.

The experimental findings and their comparison to other literature experimentation and values obtained from the predictive models are illustrated in Table 3. The size data obtained using the zetasizer measurements in this study are similar to those obtained by Singh et al. [25] and Bowen and Mohammad [26] for molecular weights below 1000, thus suggesting that the zetasizer is providing accurate sizing data within this range. However there is a significant disparity between the data obtained by Combe et al. [24] and the zetasizer values obtained in this study. The experimental data was then compared to the predictive models and was most accurately predicted by the model of Bowen and Mohammad [26] over the whole range of PEGs studied. For example the average difference between the experimentally derived values in this work and the values obtained by Coombe et al. [24], Singh et al. [25] and Bowen and Mohammad [26] is 28.1, 13.3 and 5.4% respectively. The largest discrepancy is seen for PEG 4600 where the experimentally derived radius is 1.299 nm whereas the values quoted by Oatley [14], Coombe et al. [24] and Singh et al. [25] are all greater than 1.8 nm, while Bowen and Mohammad [26] report a particle radius of 1.145 nm. Interestingly, the PEG measurements by Oatley [14] were performed on a HPPS (High Performance Particle Sizer) a predecessor of the current zetasizer equipment. As the trend of the experimental data is sensible and the vast majority of the data values concur with other values reported elsewhere in the literature, the experimentally determined values for PEG sizes were deemed acceptable and used in all subsequent calculations.

4.2 Membrane Pore Size

The accurate measurement of pore sizes in nanofiltration membranes is an area of contention, although a variety of methods have been used to measure the membrane pore size. These include AFM [27], neutral solute rejection [28], liquid-liquid displacement [29] and BET [20]. This study used three different independent measurement methods in order to estimate the membrane pore size, namely AFM, BET and neutral solute rejection. The membrane used in this study is reported by the manufacturer to have a molecular weight cut-off (MWCO) of 4000, although due to differing determination methods for each manufacturer the calculation of membrane separation characteristics is not accurate from MWCO alone.

Neutral Solute Rejection*:* The experimental approach undertaken allowed the estimation of membrane MWCO using the rejection data obtained for the PEGs studied. Membrane MWCO is often estimated using the molecular weight at which 90% of the solute is rejected. Figure 4 represents the real rejection of the PEGs studied plotted against molecular weight. The lines plotted on the figure represent the fitting of the exponential rise to maximum expression (eqn. 34). Figure 4 shows that at 2900 Da more than 90 % of the solute is rejected at all pressures studied suggesting that the 4000 MWCO claimed by the manufactures is an overestimation. Using the particle size correlation of Bowen and Mohammad [26] (37) and assuming the presence of perfectly cylindrical pores, a MWCO of 2900 (90% rejection value) gives a pore diameter of 2.06 nm. The data shown in Figure 4 shows that with increasing pressure the apparent MWCO decreases, illustrating that a quoted MWCO is highly dependent on the characterisation conditions used.

AFM measurements*:* A topographic AFM image of the Nadir UH004 membrane is shown in Figure 5. The membrane has a relatively low roughness (scan size 0.5 μm^2) of 0.4 ± 0.012 nm. The data obtained from the AFM measurements counted 1195 pores and suggests an average pore radius of

1.29 nm, with a minimum pore size measurement of 0.55 nm and a maximum measured pore size of 2.02 nm. The membrane porosity is calculated as 2.48%.

***BET measurement**:* The nitrogen adsorption-desorption isotherm of the membrane studied is illustrated in Figure 6a. The isotherm obtained in this experimental work shows a slight disparity between the adsorption and desorption isotherms. This discrepancy was observed in all experimental BET runs undertaken regardless of the mass of membrane placed in the equipment and the phenomenon is attributed to the effect that the membrane support layer has on the adsorption/desorption performance of the BET machine. The shape of the isotherm is analogous to that observed by Fang et al. [20] although in this case the maximum volume obtained at P/P0 = 1 is 4 cc g^{-1} rather than 15 cc g^{-1}, indicating that the UH004 membrane has lower surface area (i.e. larger pores) than the FO membrane used in their study (pore size = 0.25 nm). Application of the Horvath-Kawazoe method to determine the pore-size suggests a membrane pore radius for the UH004 membrane of 0.86 nm and is in the expected range for a membrane at the loose end of NF. Furthermore the pore size obtained is similar to the pore-size obtained by the AFM measurement. The pore size distribution obtained from the nitrogen adsorption-desorption isotherm is shown in Figure 6b and suggests that there are no pores larger than 0.97 nm and no pores smaller than 0.3 nm. The difference in pore size distribution determined using the BET method from the AFM method is attributed to natural variance expected between the two methodologies for measurements at nanometre length scales.

The data obtained from the independent pore size measurements suggest a pore size in the region of 1 nm (solute rejection ~1.03 nm, AFM ~1.29nm and BET ~0.86nm) is appropriate for the UH004 membrane. For this reason, a specific pore size of 1.075 nm will be used for all further calculations. This is the average of the mean pore size obtained from each of the three characterisation methods and is deemed to be representative of the actual membrane pore size distribution.

4.3 Rejections and hindrance factors

The observed rejection plotted against applied pressure for the various PEG solutions is shown in Figure 7a. The data obtained shows that PEG rejection increases with increasing PEG molecular weight as would be expected. For example, PEG 200 shows almost zero observed rejection, i.e. PEG fully transported across membrane, while PEG 4600 shows almost total rejection (100 %). However, in all cases, as the applied pressure increases beyond ~10 bar the PEG rejection dramatically decreases. For instance PEG 3400 displays a rejection of ~90% at low pressure and at 10 bar begins to fall to a minimum observed rejection of ~10% at 30 bar. This reduction in observed rejection is a result of concentration polarisation and is increasing with increasing applied pressure leading to higher membrane flux [30]. Figure 7b shows the real rejection (calculated using eqn. 31) plotted against applied pressure. The lines plotted on Figure 7b are the statistical regression of the data using eqn. (34) allowing the determination of the limiting rejection. Similarly to Figure 7a, PEG rejection increases with increasing molecular weight. PEG 200 is seen to have the minimal rejection of all the PEGs studied as expected and reaches a maximum rejection of ~5% at 30 bar. The effect of increasing pressure is seen to increase rejection in the majority of PEGs studied; this effect is particularly profound in PEGs 400, 600, 1000, 1450, 2000 and sucrose. PEGs 3400 and 4600 display almost constant rejection over the total pressure range studied with all rejections above 90%. Figure 7b indicates that the lower molecular weight species, PEG 200, PEG 400 and sucrose, do not achieve

limiting rejection over the pressure range studied. So in the case of these three species, the limiting rejection was taken as the real rejection at the highest applied pressure. The result observed for PEG 400 is particularly strange in that the real rejection is seen to be above that of PEG 600 suggesting that some of the results obtained for PEG 400 are anomalous. The statistical curve fitting for all other solutes measured suggests that the rejection has reached the limiting value and this maximum value was then used in subsequent calculations. The data points for the limiting rejection were then plotted against measured particle size and are illustrated as Figure 7c. The limiting rejection increases with increasing particle size and rises to a maximum as expected. The values from Figure 7c, along with eqn. (28), were then used to calculate the convective hindrance factors K_c and these are shown in Figure 8. The experimentally determined values for Kc from the PEG 400, 600, 1000 and 1450 are in close agreement to the theoretical data. The Kc value obtained for PEG 200 deviates away from the theoretical prediction and this is attributed to the fact that limiting rejection has not been achieved for this species. A sensitivity analysis conducted into the magnitude of the limiting rejection value used for these species showed that a reduction of pore radius to 0.8 nm results in the calculated Kc values to increase and in some cases more than double, creating a significant disparity between the experimentally derived and theoretical values. An increase in pore radius to 1.2 nm results in the experimentally derived Kc values decreasing to below the theoretical line.

Once the convective hindrance factors were obtained, the diffusive hindrance factors could then be calculated from the rejection profile over the range of pressure using eqn. (27) and the derived values for pore size and particle size. The experimental value for the diffusive hindrance factor is also plotted in Figure 8. As for the convective hindrance factors, the results obtained for the diffusive hindrance factors are similar in magnitude to those values obtained from the finite element methods. The values do deviate away from the theoretically predicted line and exhibit a pseudo linear relationship. Interestingly, performing the same sensitivity analysis by varying the pore size in a similar fashion to that used previously for the convective hindrance factors results in very little variation of the K_d value. When considering the assumptions included in the development of hydrodynamic descriptions and the inherent experimental errors involved in this work, these experimental results provide reassurance in the validity of the theoretical descriptions of these complex hydrodynamic phenomena and suggest that the currently accepted models derived for microfiltration and ultrafiltration do provide an accurate prediction of the hindrance factors and are suitable for use in NF applications.

5.0 Conclusion

This study has successfully used the rejection experiments of neutral solutes to determine the hindrance factors involved in the transport of materials through an NF membrane. To the best of the author's knowledge the experimental determination of such hydrodynamic forces for a nano scale membrane has not been conducted previously. The work confirms that the hydrodynamic forces are highly dependent on the ratio of solute to pore size. Three independent methods (neutral solute rejection, AFM and BET) were used to determine the pore size of the Nadir UH004 membrane and the average pore size was taken to be 1.075 nm. The particle size for a series of PEGs was independently determined using dynamic light scattering. This information along with a series of rejection profiles was used then used to experimentally determine both the convective and diffusive

hindrance factors. The values obtained were deemed sensible and were compared to calculated point values obtained from hydrodynamic theory using finite element methods. Both sets of data were similar and the experimental values for hindrance factors were shown to be a fair representation of the theoretical data. This suggests that the correlations found throughout the literature are accurate enough for the calculation of the hindrance factors describing the hydrodynamic forces experienced by a solute in a nanopore.

6.0 Acknowledgment

This work is part-funded by the European Social Fund (ESF) through the European Union's Convergence programme administered by the Welsh Government and EnAlage.

References

[1] E. Bringas, M.F. San Román, J.A. Irabien, I. Ortiz, An overview of the mathematical modelling of liquid membrane separation processes in hollow fibre contactors, J. Chem. Technol. Biotechnol. 84 (2009) 1583–1614.

[2] A.I. Schafer, A.G. Fane, T.D. Waite, Nanofiltration: Principles and Applications, Elsevier, London, 2005.

[3] W.J. Lau, A.F. Ismail, N. Misdan, M.A. Kassim, A recent progress in thin film composite membrane: A review, Desalination. 287 (2012) 190 – 199.

[4] W.R. Bowen, H. Mukhtar, Characterisation and prediction of separation performance of nanofiltration membranes, J. Membr. Sci. 112 (1996) 263 – 274.

[5] W.M. Deen, Hindered Transport of Large Molecules in Liquid-Filled Pores, AlChE J. 33 (1987) 1409 – 1425.

[6] P.L. Paine, P. Scherr, Drag coefficients for the movement of rigid spheres through liquid-filled cylindrical pores, Biophys J. 15 (1975) 1087 – 1091.

[7] M.G. Davidson, W.M. Deen, Hindered diffusion of water-soluble macromolecules in membranes, Macromolecules. 21 (1988) 3474 – 3481.

[8] J. Koh, P.C. Wankat, N.H.L. Wang, Pore and surface diffusion and bulk-phase mass transfer in packed and fluidized beds, Ind. Eng. Chem. Res. 37 (1998) 228-239.

[9] W.R. Bowen, A.O. Sharif, Transport through microfiltration membranes – Particle hydrodynamics and flux reduction, J. Colloid and Interface Sci. 168 (1994) 414-421.

[10] M. Kim, A.L. Zydney, Effect of electrostatic, hydrodynamic, and Brownian forces on particle trajectories and sieving in normal flow filtration, J. Colloid and Interface Sci. 269 (2004) 425-431.

[11] V. Silva, P. Pradanos, L. Palacio, J.I. Calvo, A. Hernandez, Relevance of hindrance factors and hydrodynamic pressure gradient in the modelization of the transport of neutral solutes across nanofiltration membranes, Chem. Eng. J. 149 (2009) 78-86.

[12]P. Dechadilok, W.M. Deen, Hindrance factors for diffusion and convection in pores, Ind. Eng. Chem. Res. 45 (2006) 6953 – 6959.
[13]W.R. Bowen, A.W. Mohammad, N. Hilal, Characterisation of nanofiltration membranes for predictive purposes – Use of salts, uncharged solutes and atomic force microscopy, J. Membr. Sci. 126 (1997) 91 – 105.
[14]D.L. Oatley, Characterisation and prediction of membrane separation performance – An industrial assessment, PhD Thesis (2004) University of Wales Swansea, UK.
[15]W.R. Bowen, J.S. Welfoot, Modelling the performance of membrane nanofiltration – critical assessment and model development, Chem. Eng. Sci. 57 (2002) 1121-1137.
[16]D.L. Oatley-Radcliffe, S.R. Williams, C. Lee, P.M. Williams, Mass transfer characterisation of three commercial frontal filtration membrane systems, J. Membr. Sci. (2014) – Submitted
[17]British Standards Institution, BS 3406-8: Methods for Determination of particle size distribution – Part 8: Photon correlation spectroscopy (1997) London: BSI.
[18]J.I. Calvo, A. Hernández, P. Prádanos, L. Martinez, W.R. Bowen, Pore size distributions in microporous membranes, J. Colloid and Interface Sci. 176 (1995) 467 – 468.
[19]P. Prádanos, M.L. Rodriguez, J.J. Calvo, A. Hernández, F. Tejerina, J.A. de Saja, Structural characterization of an UF membrane by gas adsorption-desorption and AFM measurements, J. Membr. Sci. 117 (1996) 291 – 302.
[20]Y. Fang, L. Bian, Q. Bi, Q. Li, X. Wang, Evaluation of the pore size distribution of a forward osmosis membrane in three different ways, J. Membr. Sci. 454 (2014) 390 – 397.
[21]A.W. Mohammad, N. Hilal, H. Al-Zoubi, N.A. Darwish, Prediction of permeate fluxes and rejections of highly concentrated salts in nanofiltration membranes, J. Membr. Sci. 289 (2007) 40 – 50.
[22]S. Nicolas, B. Balannec, F. Beline, B. Bariou, Ultrafiltration and reverse osmosis of small non-charged molecules: a comparison study of rejection in a stirred and unstirred batch cell, J. Membr. Sci.164 (2000) 141-155.
[23]S. Nakao, S. Kimura, Analysis of solutes rejection in ultrafiltration, J. Chem. Eng. Jpn. 14 (1981) 32-37.
[24]C. Combe, E. Molis, P. Lucas, R. Riley, M.M. Clark The effect of CA membrane properties on adsorptive fouling by humic acid, J. Membr. Sci. 154 (1999) 73 – 78.
[25]S. Singh, K.C. Khulbe, T. Matsuura, P. Ramamurphy, Membrane characterisation by solute transport and atomic force microscopy, J. Membr. Sci. 142 (1998) 111 – 127.
[26]W.R. Bowen, A.W. Mohammad, Characterisation and prediction of nanofiltration membrane performance – a general assessment, Chem. Eng. Res. Des. 76 (1998) 885-893.
[27]N. Hilal, H. Al-Zoubi, N.A. Darwish, A.W. Mohammad, M.A. Arabi, A comprehensive review of nanofiltration membranes: Treatment, pretreatment, modelling, and atomic force microscopy, Desalination. 170 (2004) 281 – 308.
[28]N. Garcia-Martin, V. Silva, F.J. Carmona, L. Palacio, A. Hernandez, P. Pradanos, Pore size analysis for retention of neutral solutes through nanofiltration membranes. The contribution of concentration-polarisation, Desalination. 344 (2014) 1 – 11.
[29]J.A. Otero, O. Mazarrasa, J. Villasante, V. Silva, P. Pradanos, J.I. Calvo, A. Hernandez, Three independent ways to obtain information on pore size distributions of nanofiltration membranes, J. Membr. Sci. 309 (2008) 17 – 27.

[30]D.L. Oatley, L. Llenas, R. Perez , P.M. Williams, X. Martínez-Lladó, M. Rovira, Review of the dielectric properties of nanofiltration membranes and verification of the single oriented layer approximation, Adv. Colloid Interface Sci. 173 (2012) 1-11.
[31] J.L. Anderson, J.A. Quinn, Restricted transport in small pores, Biophys. J. 14 (1974) 130.
[32]J.L. Anderson, J.A. Quinn, Ionic mobility in microcapillaries. A test for anomalous water structures, Journal of the Chemical Society, J. Chem. Soc., Faraday Trans. 1. 68 (1972) 744 – 748.
[33]H. Brenner, L.J. Gaydos, The constrained Brownian movement of spherical particles in cylindrical pores of comparable radius, J. Colloid and Interface Sci. 58 (1977) 312 – 356.
[34]S. Bandini, D. Vezzani, Nanofiltration modelling: the role of dielectric exclusion in membrane characterization, Chem. Eng. Sci. 58 (2003) 3303 – 3326.
[35]G.M. Mavrovouniotis H. Brenner, Hindered sedimentation and dispersion coefficients for rigid closely fitting Brownian spheres in circular cylindrical pores containing quiescent fluids, AIChE annual meeting (1987) Paper 85b. Adapted from: V. Silva, P. Pradanos, L. Palacio, A. Hernandez, Alternative pore hindrance factors: What one should be used for nanofiltration modelization?, Desalination. 245 (2009) 606 – 613.
[36]W.L. Haberman, R.M. Sayre, Motion of Rigid and Fluid Spheres in Stationary and Moving Liquids Inside Cylindrical Tubes, David Taylor Model Basin, Report N^{o} 1143, U.S. Navy, Washington D.C. (1958).
[37]P.M. Bungay, H. Brenner, The motion of a closely fitting sphere in a fluid-filled tube, Int. J. Multiphase Flow, 1, (1973), 25 – 56.
[38]G. Horvath, K Kawazoe, Method for the Calculation of Effective Pore Size Distribution in Molecular Sieve Carbon, J. Chem. Eng. Japan, 16 (5), (1983), 470-475.
[39]R.W. Magee, Evaluation of the External Surface Area of Carbon Blacks by Nitrogen Adsorption, Presented at the Meeting of the Rubber Division of the American Chem. Soc., October, 1994.
[40]J.H. de Boer, B.G. Linsen, Th. van der Plas, G.J. Zondervan, Studies on pore systems in catalysts: VII. Description of the pore dimensions of carbon blacks by the t method, J. Catalysis, 4, (1965), 649-653.

Figures

Figure 1: Schematic diagram of the movement of a rigid spherical solute inside a perfectly cylindrical pore.

Figure 2: Raw data for diffusive and convective pore hindrance factors proposed in the literature along with the polynomial fitting of Oatley (2004) [14] as an example.

Figure 3: A schematic diagram of the dead-end filtration equipment. (1) nitrogen cylinder, (2) valve, (3) feed reservoir, (4) pressure sensor, (5) water bath, (6) Membrane cell, (7) magnetic stirrer, (8) electronic balance, (9) PC.

Figure 4: PEG rejection with varying molecular weight from the Nadir UH004 membrane.

Figure 5: Topographic AFM image of the Nadir 4000 MWCO membrane

Figure 6: a) BET Nitrogen adsorption/desorption isotherm for the Nadir UH004 membrane, b) BET pore size distribution

Figure 7: PEG rejection from the Nadir UH004 membrane with applied pressure
(a) observed rejection and (Dotted line for illustrative purposes only) (b) real rejection (c) Limiting real rejection against measured particle size (sucrose data obtained from Bowen and Mohammad [26])

Figure 8: Experimentally derived hindrance factors (pore radius: 1.075 nm)

Table 1: Point values for hindrance factors determined by finite element methods. The values reported for $\lambda \leq 0.4$ are the original data from Anderson and Quinn [31], and the additional values are obtained from Oatley [14].

Table 2: Theoretical descriptions for the convective (K_c) and diffusive (K_d) hydrodynamic coefficients.

Table 3: Measured sizing data for PEG from the Zetasizer compared with other experimental and theoretical values. *values from this study.

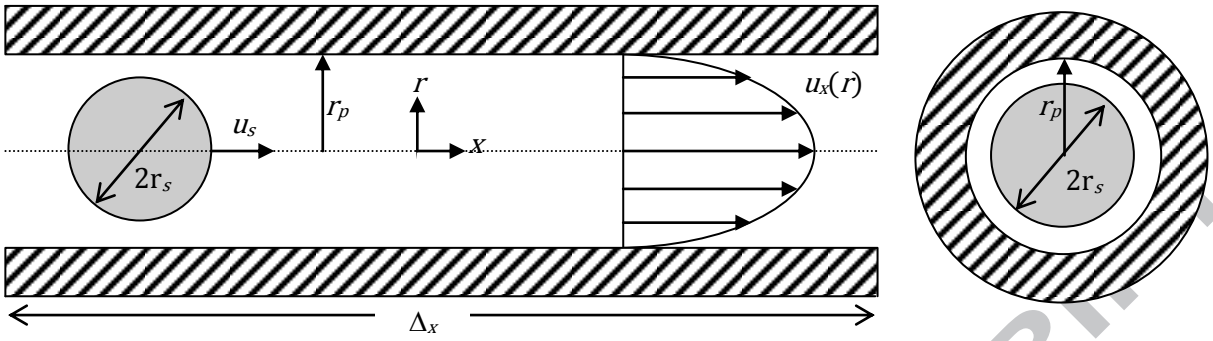

Figure 1

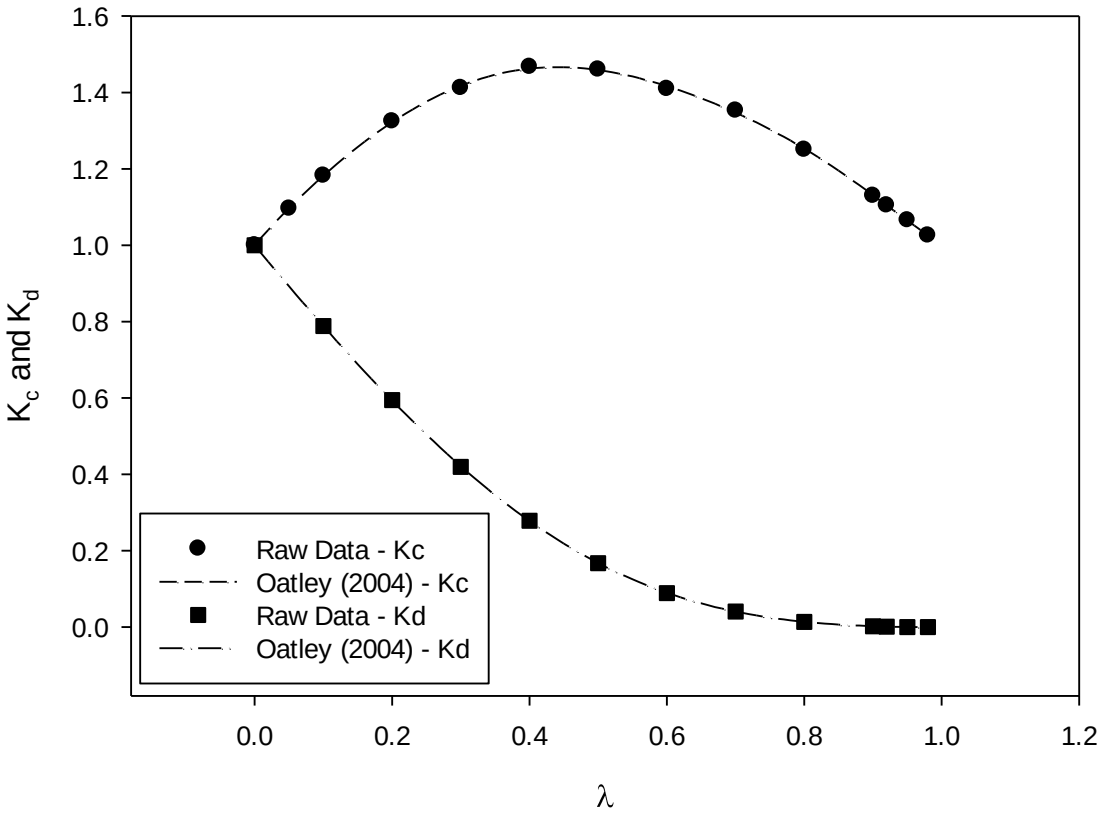

Figure 2

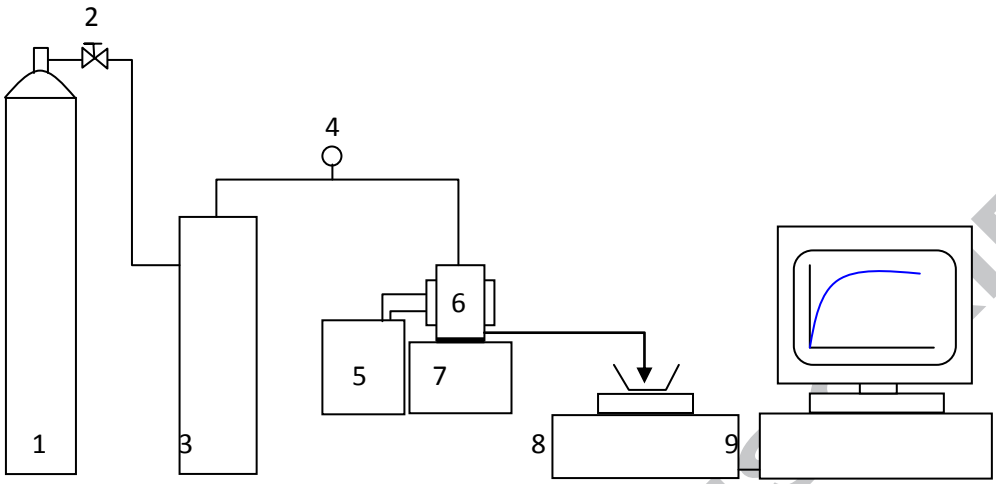

Figure 3

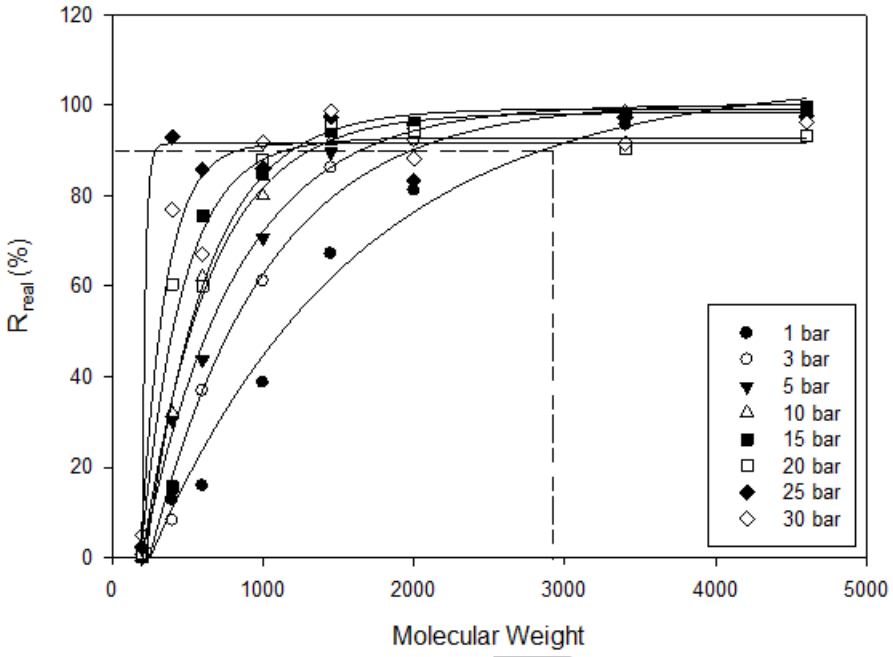

Figure 4

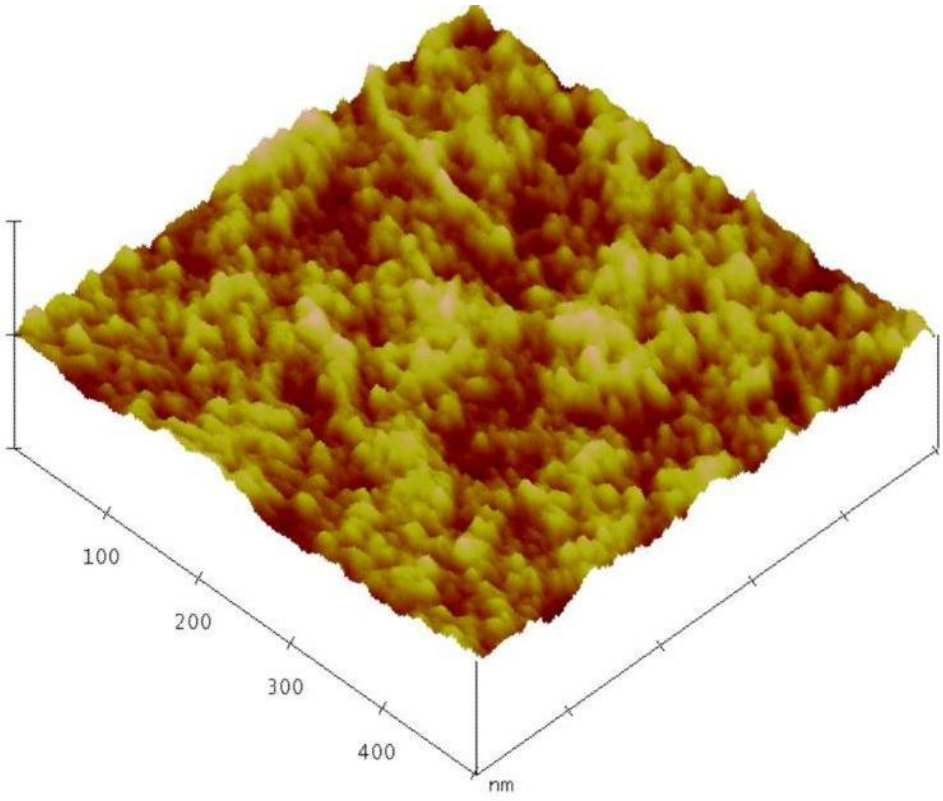

Figure 5

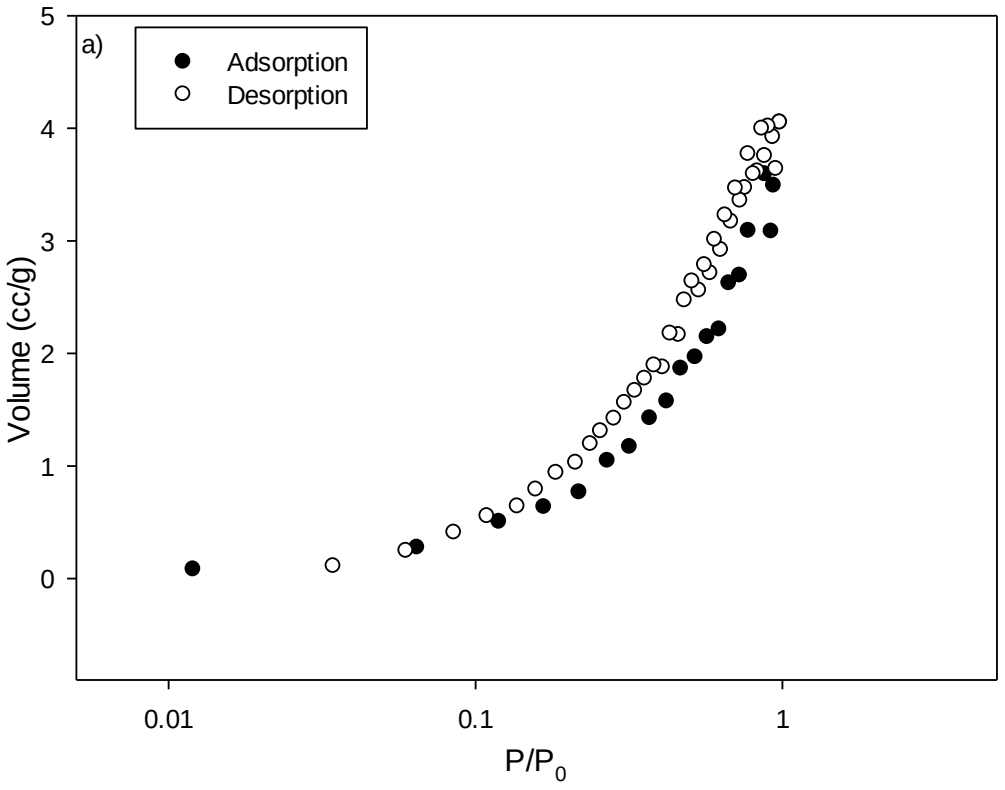
a)
Adsorption
Desorption
Volume (cc/g)
0
1
2
3
4
5
0.01
0.1
1
P/P0

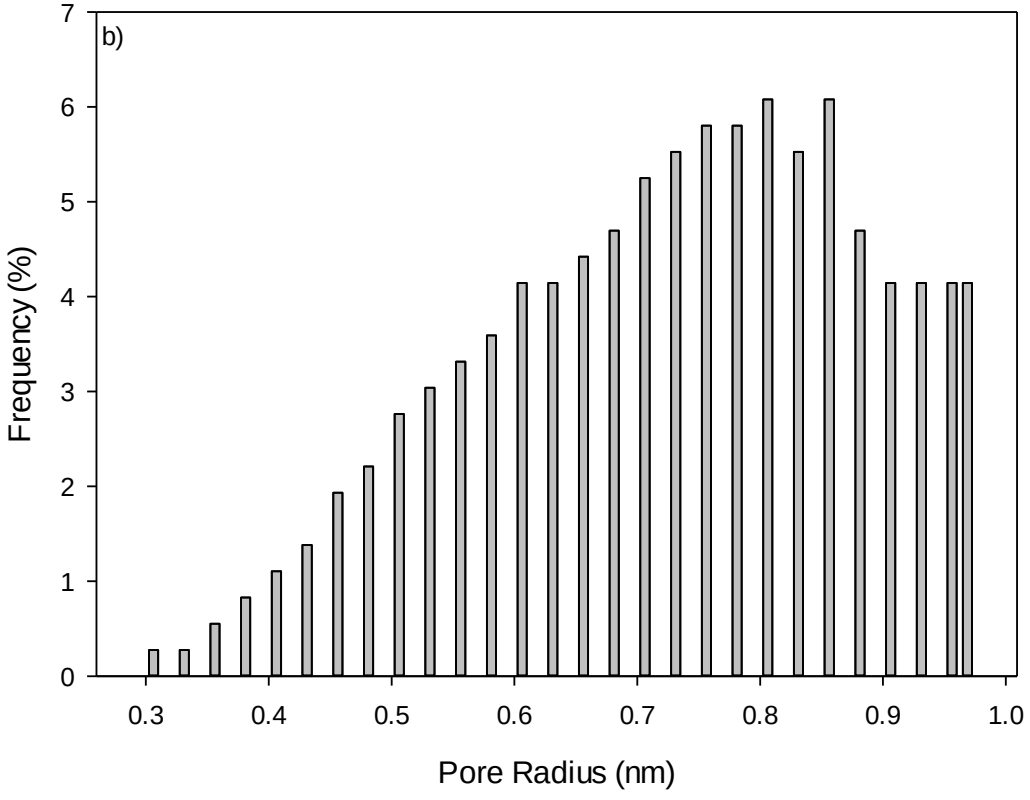
b)
Frequency (%)
0
1
2
3
4
5
6
7
0.3
0.4
0.5
0.6
0.7
0.8
0.9
1.0
Pore Radius (nm)

Figure 6

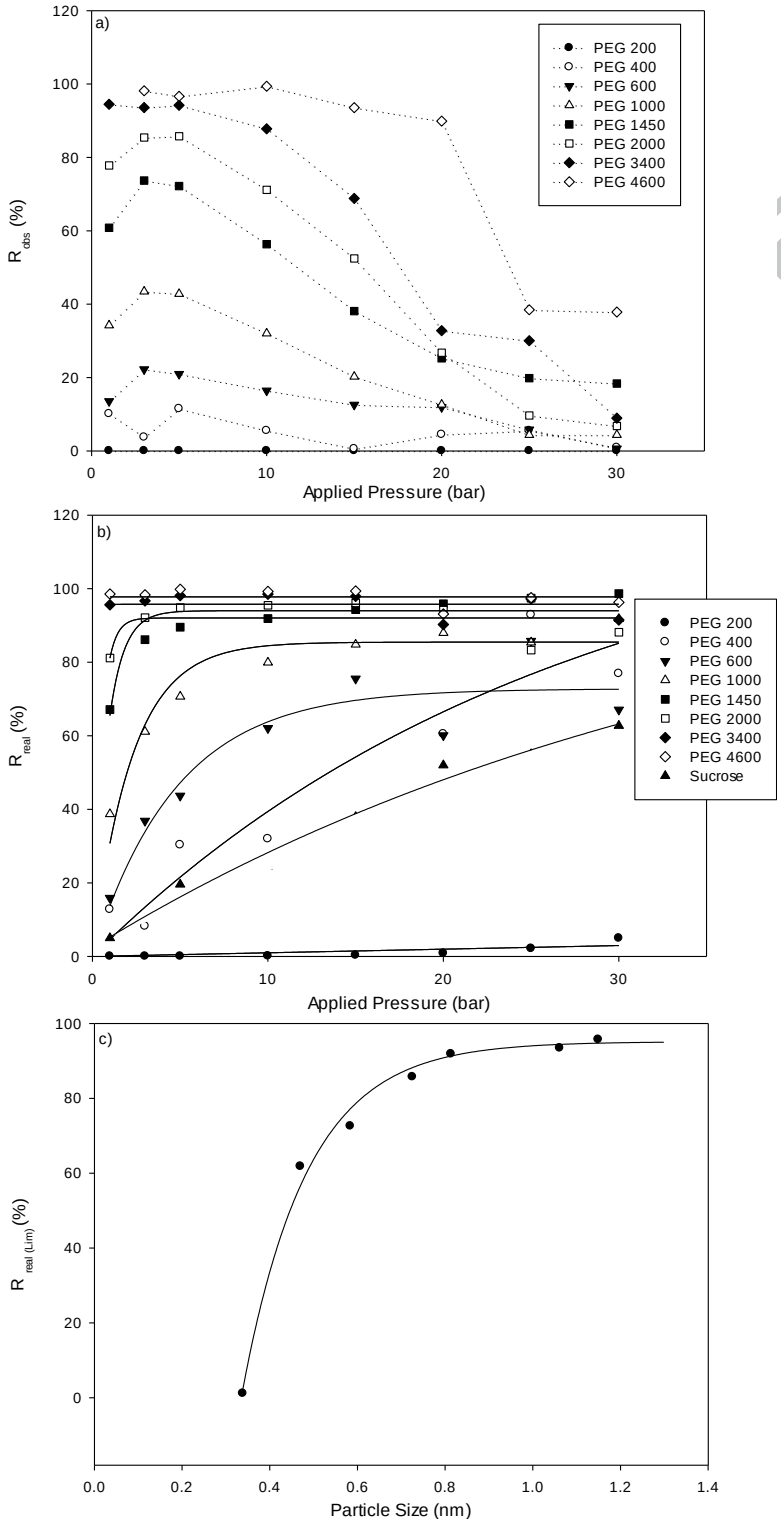
a)
PEG 200
PEG 400
PEG 600
PEG 1000
PEG 1450
PEG 2000
PEG 3400
PEG 4600
R dts (%)
Applied Pressure (bar)
b)
PEG 200
PEG 400
PEG 600
PEG 1000
PEG 1450
PEG 2000
PEG 3400
PEG 4600
Sucrose
R real (%)
Applied Pressure (bar)
c)
R real (Lim) (%)
Particle Size (nm)

Figure 7

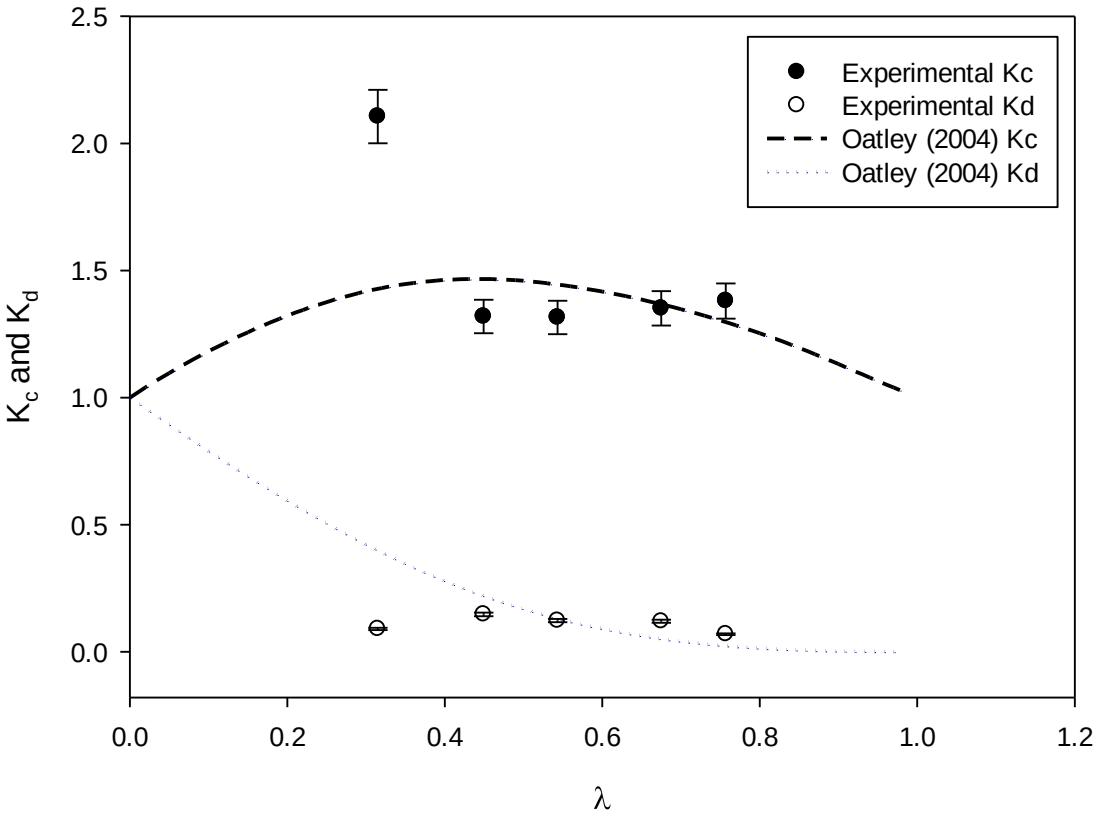

Figure 8

λ	K^1	G	Φ	$K_{i,c}$	$K_{i,d}$
0	1	1	1	1	1
0.05	0.8950	0.9983	0.9025	1.09565	0.89504
0.10	0.7916	0.9932	0.8100	1.18187	0.79164
0.20	0.5955	0.9720	0.6400	1.32196	0.59553
0.30	0.4228	0.9356	0.4900	1.41275	0.42278
0.40	0.2822	0.8829	0.3600	1.44796	0.28223
0.50	0.1673	0.8343	0.2500	1.46009	0.16734
0.60	0.0892	0.7660	0.1600	1.40946	0.08918
0.70	0.0407	0.7081	0.0900	1.35256	0.04067
0.80	0.0134	0.6379	0.0400	1.25032	0.01345
0.90	0.0021	0.5676	0.0100	1.12951	0.00213
0.92	0.0012	0.5540	0.0064	1.10447	0.00119
0.95	0.0004	0.5335	0.0025	1.06561	0.00035
0.98	0.0000	0.5128	0.0004	1.02531	0.00003

Table 1

Model	Equation	Range	Reference
Anderson and Quinn	$K_d = 1 - 2.1044\lambda + 2.089\,\lambda^3 - 0.948\,\lambda^5$ $K_c = (1 + 2\lambda - \lambda^2)(1 - (2/3)\,\lambda^2 - 0.163\,\lambda^3)$	$0 < \lambda \leq 0.4$	[32]
Brenner and Gaydos	$K_d = \frac{1 - (9/8)\lambda \ln \lambda^{-1} - 1.539\lambda}{1 - 2\lambda + \lambda^2}$ $K_c = (1 + 2\lambda - 4.9\lambda^2)$	$0 < \lambda \leq 0.1$	[33]
Bowen and Sharif	$K_d = -1.705\lambda + 0.946$ $K_c = (-0.301\lambda + 1.022)\,(1+2\lambda - \lambda^2)$	$0 < \lambda \leq 0.4$	[9]
Bowen et al.	$K_d = 1 - 2.3\lambda + 1.154\lambda^2 + 0.224\lambda^3$ $K_c = (1 + 0.054\lambda - 0.988\lambda^2 + 0.441\lambda^3)(1+2\lambda - \lambda^2)$	$0 < \lambda \leq 0.8$	[13]
Bandini and Vezanni	$K_d = -0.105 + 0.318\lambda - 0.213\lambda^2$ $K_c = (-6.830 + 19.348\lambda - 12.518\lambda^2)(1+2\lambda - \lambda^2)$	$0.8 < \lambda \leq 1$	[34]
Mavrovouniotis and Brenner	$K_d = \frac{0.984(1 - \lambda)^{9/2}}{1 - 2\lambda + \lambda^2}$	$\lambda > 0.9$	[35]
Haberman and Sayre	$K_d = \frac{1 - 2.105\lambda + 2.0865\lambda^3 - 1.7068\lambda^5 + 0.7260\lambda^6}{1 - 0.75857\lambda^5}$ $K_c = \frac{(1 + 2\lambda - \lambda^2)(1 - (2/3)\lambda^2 - 0.20217\lambda^5)}{1 - 0.75857\lambda^5}$	$0 < \lambda \leq 0.9$	[36]
Oatley	$K_d = 1 - 2.1812\lambda + 0.7328\lambda^2 - 0.9065\lambda^3 + 6.7272\lambda^4 - 10.2324\lambda^5 + 6.3293\lambda^6 - 1.4692\lambda^7$ $K_c = (1+ 2\lambda - \lambda^2)(1 + 0.0650\lambda - 1.9370\lambda^2 + 8.5211\lambda^3 - 27.3398\lambda^4 + 44.4150\lambda^5 - 34.4150\lambda^6 + 10.3358\lambda^7)$	$0 < \lambda \leq 0.98$	[14]
Dechadilok and Deen	$K_d = \frac{1}{1 - \lambda^2}\left(1 + \frac{9}{8}\lambda \ln \lambda - 1.5603\lambda + 0.52815\lambda^2 + 1.9152\lambda^3 - 2.8190\lambda^4 + 0.27078\lambda^5 + 1.10115\lambda^6 - 0.43593\lambda^7\right)$ $K_c = \frac{1 + 3.867\lambda - 1.907\lambda^2 - 0.834\lambda^3}{1 + 1.867\lambda - 0.741\lambda^2}$	$0 < \lambda \leq 0.95$	[12]
Bungay and Brenner	$K_d = \frac{6\pi}{K_t} \quad K_c = (1 + 2\lambda - \lambda^2)\frac{K_s}{2K_t}$ $K_t = \frac{9}{4}\pi^2\sqrt{2}(1 - \lambda_i)^{-5/2}\left(1 + \sum_{n=1}^{2} a_n (1 - \lambda_i)^n\right) + \sum_{n=0}^{4} a_{n+3}\lambda_i^n$ $K_s = \frac{9}{4}\pi^2\sqrt{2}(1 - \lambda_i)^{-5/2}\left(1 + \sum_{n=1}^{2} b_n (1 - \lambda_i)^n\right) + \sum_{n=0}^{4} b_{n+3}\lambda_i^n$	$0 < \lambda \leq 1$	[37]

a_1	a_2	a_3	a_4	a_5	a_6	a_7
-1.2167	1.5336	-22.5083	-5.6117	-0.3363	-1.216	1.647
b_1	b_2	b_3	b_4	b_5	b_6	b_7
0.1167	-0.0442	4.018	-3.9788	-1.9215	4.392	5.006

Table 2

	Measurements			Theoretical	
	DLS Measurements		PEG diffusion measurements	Stokes-Einstein of PEGs	Known values of small solutes
Molecular Weight (Da)	Zetasizer* (r.nm)	Oatley [14] (r.nm)	Combe et al. [24] (r.nm)	Singh et al. [25] (r.nm)	Bowen and Mohammad [26] (r.nm)
200	0.339	-	0.463	0.32	0.374
400	0.483	-	0.628	0.471	0.491
600	0.584	-	0.751	0.59	0.577
1000	0.726	-	0.94	0.784	0.706
1450	0.814	1.11	1.107	0.965	0.817
2000	1.062	-	1.275	1.154	0.928
3400	1.149	1.75	1.611	1.551	1.138
4600	1.299	1.85	1.84	1.835	1.145

Table 3

Graphical abstract

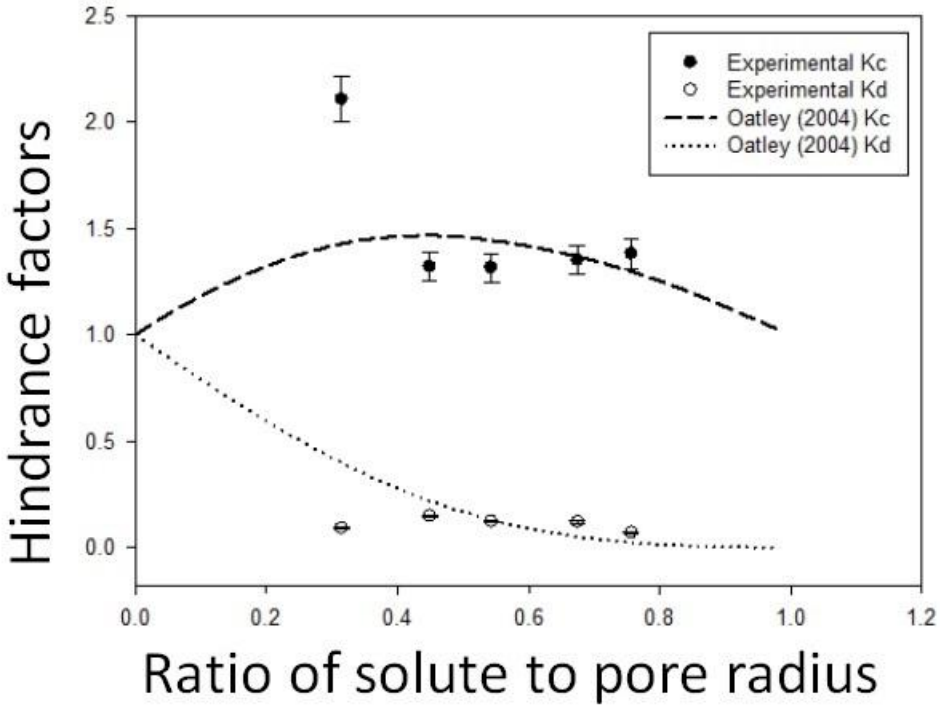

Highlights

Hindrance factors (hydrodynamic drag coefficients) have been determined experimentally for NF

Experimental hindrance factors have been compared to theoretical point values

Experimental and theoretical hindrance values are similar and validate use for NF membranes